ACS Energy LETTERS

http://pubs.acs.org/journal/aelccp

LETTER

Optically Determined Hole Effective Mass in Tin-Iodide Perovskite Films

Published as part of ACS Energy Letters special issue "The Evolving Landscape of Energy Research: Views from the Editorial Team".

Vincent J.-Y. Lim, Marcello Righetto, Michael D. Farrar, Thomas Siday, Henry J. Snaith, Michael B. Johnston, and Laura M. Herz*

Cite This: ACS Energy Lett. 2025, 10, 4589−4595

Read Online

ACCESS | Metrics & More | Article Recommendations | Supporting Information

ABSTRACT: **Tin-halide perovskites currently offer the best photovoltaic performance of lead-free metal-halide semiconductors. However, their transport properties are mostly dominated by holes, owing to ubiquitous self-doping. Here we demonstrate a noncontact, optical spectroscopic method to determine the effective mass of the dominant hole species in $FASnI_3$, by investigating a series of thin films with hole densities finely tuned through either SnF_2 additive concentration or controlled exposure to air. We accurately determine the plasma frequency from mid-infrared reflectance spectra by modeling changes in the vibrational response of the FA cation as the plasma edge shifts through the molecular resonance. Our approach yields a hole effective mass of $0.28m_e$ for $FASnI_3$ and demonstrates parabolicity within ∼100 meV of the valence band edge. An absence of Fano contributions further highlights insignificant coupling between the hole plasma and FA cation. Overall, this approach enables noncontact screening of thin-film materials for optimized charge-carrier transport properties.**

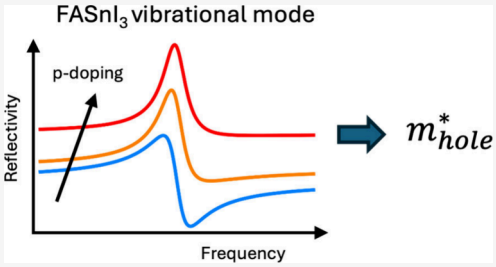

Lead-free halide perovskites have emerged as an environmentally compatible alternative to lead-halide perovskites, with potential applications ranging from photovoltaics, photocatalysis, to field-effect transistors.[1−5] In this family of materials with stoichiometry ABX_3, toxic Pb(II) B cations are replaced by isoelectronic metal cations, such as Sn(II) or Ge(II), or, in double perovskites of stoichiometry $A_2BB'X_6$, by heterovalent cation pairs, such as Ag(I)−Bi(III) or Ag(I)−Sb(III).[6,7] Beyond addressing toxicity constraints, the vast chemical space available for lead-free halide perovskites has enabled extending the bandgap engineering range for multijunction solar cell applications[8−10] and developing further emerging properties of these metal-halide semiconductors, such as photo(electro)catalytic[3] and white-light emission properties.[11] However, replacing Pb(II) cations while preserving the excellent optoelectronic properties of lead-halide perovskites[12] has proven an extraordinary challenge.[13] Limited charge-carrier transport, originating from both intrinsic (i.e., band dispersion and phonon coupling) and extrinsic (i.e., traps and grain boundaries) effects, is currently a major challenge for lead-free perovskites. Therefore, understanding the role of metal cation substitution in transport properties is critical for developing efficient lead-free perovskite materials.

Tin-halide perovskites of stoichiometry $ASnX_3$ have to-date proven to be the best-performing lead-free perovskite semiconductors by some margin, with photovoltaic conversion efficiencies in excess of 15% now having been reported.[14] Here, the halide X-site is typically chosen to be iodide (I^-) for lowest band gaps, and the A-site may be occupied by formamidinium (FA^+), methylammonium (MA^+), cesium (Cs^+), or a mixture thereof,[13,15−18] with FA being increasingly popular owing to its superior thermal stability compared with MA.[19] Early studies on pressed powders of tin iodide perovskites reported promising Hall mobilities of up to a few hundred $cm^2/(V\ s)$ but noted that these materials displayed strong p-type conduction.[15−18] Further advances in materials processing yielded thin films of high optoelectronic quality,[5,20−22] triggering implementation in devices such as solar cells[14] and light emitters, however, issues with undesirably large background hole densities remained.[23,24] Such effects ultimately arise from tin iodide perovskites exhibiting lower spin−orbit coupling than their lead-based counterparts (tin being lighter

Received: July 22, 2025
Revised: August 19, 2025
Accepted: August 20, 2025
Published: August 28, 2025

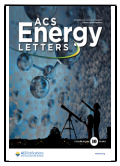

https://doi.org/10.1021/acsenergylett.5c02283
ACS Energy Lett. 2025, 10, 4589−4595

than lead),[22,25] and therefore reduced ionization energies.[26] Tin vacancies are thus easily formed,[17,26,27] which in turn creates a locally iodine-rich environment that promotes the oxidation of Sn^{2+} to Sn^{4+} and chemical conversions e.g. to SnO_2 or SnI_4.[26,27] Such links between tin vacancy formation, tin oxidation and chemical conversion unfortunately also open routes to material decomposition in air and water.[19,28] From an electronic perspective, tin vacancies generate defect levels close to the valence band edge[26] which effectively capture and extract electrons from the valence band, generating high hole densities[15,20,29] often in excess of 10^{18} cm^{-3}. Such excess holes may rapidly recombine with any photogenerated electrons and limit mobilities through the introduction of additional scattering processes. Significant advances in tin-halide perovskite processing have been made to minimize such unintentional self-doping, based e.g. on the use of additives to act as reducing agents or tin sources, control of crystallization, or partial ion substitution.[30,31] The most popular strategy has been the use of SnF_2 additive[13,29,32] to create a Sn-rich environment that suppresses tin vacancy formation. However, despite such efforts, the optoelectronic properties of tin-halide perovskites ultimately still remain dominated by a single charge-carrier species: holes in the valence band.

While charge-carrier recombination and transport has been much examined in thin films of tin-halide perovskites,[20,32,33] more fundamental material parameters, such as the values of the individual electron and hole effective masses, remain under debate. Experimentally, individual electron or hole masses can be hard to determine from all-optical measurements best suited to the investigation of thin films. Magneto-optical studies yielding values for reduced electron−hole masses have been widely applied to metal halide perovskites,[34] including some mixed lead−tin iodides,[35] but measurements for tin-only perovskites have been challenging. Optical measurements on tin-only halide perovskite films have generally been hampered by the effects of self-doping which causes very broad absorption spectra, as well as film inhomogeneity that causes strong light scattering, and material instability reducing data acquisition times.[35] From a theoretical perspective, the charge-carrier effective masses are inversely proportional to the calculated curvature of the electronic bands, with relativistic effects playing a role.[13] For tin-iodide perovskites, the homovalent replacement of Pb(II) with Sn(II) cations—which have an analogous electronic ns^2 configuration—preserves the high electronic dimensionality (i.e., the connectivity of the orbitals comprising the band edges) of the material. Here, the Sn−I bond lies at the heart of the tin iodide perovskite: on the one hand, the conduction band comprises antibonding Sn 5p − I 5p orbitals, while on the other hand, the valence band is comprised of the hybridized antibonding orbitals from Sn 5s and I 5p states.[13,36] First-principles calculations from Umari et al. have shown that the shallower and more active Sn $5s^2$ lone-pair states (with respect to the Pb $6s^2$ lone-pair states) yield more dispersive valence bands.[22] However, theoretical computational studies have reported a surprisingly wide range of values for the effective masses of electrons and holes. While some studies report moderate values between 0.1 and $0.3m_e$, where m_e is the electron rest mass,[22,37−39] others extend from as low as 0.05 to as high as $1.03m_e$.[36,40,41] Therefore, despite the dominance of holes in tin halide perovskite films, an accurate determination of their masses remains elusive.

In this Letter, we provide an accurate determination of the hole effective mass for the archetypal tin-halide perovskite, $FASnI_3$, by deploying a noncontact optical spectroscopic method to a series of $FASnI_3$ thin films with different background hole densities. Specifically, we deduce the hole mass from a novel approach that extracts the plasma frequency accurately from mid-infrared reflectance spectra, by modeling changes in the vibrational response of the FA cation as the plasma edge shifts through its line shape with increased background hole density. To ensure high accuracy of mass determination, we utilize changes in SnF_2 additive concentration during film fabrication as well as subsequent timed air exposure in order to vary the hole density across a wide range of values, monitored by noncontact THz conductivity measurements. Our approach yields a hole effective mass of $0.28m_e$ for $FASnI_3$ and further establishes a near-parabolic valence band up to energies of at least 100 meV above the band edge. This approach demonstrates the power of an optical approach toward determining individual charge-carrier masses in thin films for photovoltaic applications, which will aid the rapid design and exploration of materials with optimized charge-carrier transport.

We investigated a series of $FASnI_3$ thin films deposited onto z-cut quartz substrates, with the initial background density of holes being controlled by tuning the concentration of the SnF_2 additive in the precursor solution before spin-coating onto z-cut quartz (Supporting Information (SI) Section 1). We determined the hole density across the thin-film series by measuring the thin-film conductivity spectra of the films by means of terahertz-time domain spectroscopy (THz-TDS), displayed in Figure 1a and SI Figures S2 and S3. We assumed a comparatively negligible dopant density for $FASnI_3$ thin films with 20% SnF_2 additive, for which the measured THz spectrum is predominantly associated with the broad absorption peaks of tin-halide optical phonon modes, as reported earlier.[32] As the SnF_2 concentration was reduced from 20% to 0%, we observed a significant increase in the film conductivity σ_{dark} (Figure 1a), as a result of the additional free hole density arising from self-doping. We find increasing SnF_2 concentration is associated with general improvements in optoelectronic film quality (see e.g. Figure S4 in SI) in agreement with other studies highlighting beneficial effects of SnF_2 addition up to 20%.[42−44] As shown previously,[28,32] we are able to convert such dark conductivity values to background hole densities in combination with measurements of the THz mobility determined through the optical-pump terahertz-probe (OPTP) technique (Figure S4)—see SI Section 2.3 for further details. The hole mobility μ_h was determined from the THz mobility value obtained from OPTP (Figure S4) based on comparable electron and hole mobilities[22,45] and the hole density p determined via the equation $\sigma_{dark} = pe\mu_h$. The resulting hole density values for the thin-film series (Figure 1b) show a monotonic increase in doping density with decreasing SnF_2, and fall into a density regime where holes exist as free charge carriers.[46] In addition, we were able to achieve finer steps in hole density by controlled exposure of the films to ambient air for discrete amounts of time, which further increase the p-doping in the material, as can be seen in Figure 1c.[28]

For a bulk semiconductor, a conventional and straightforward method of measuring the effective mass of a single charge carrier can be the measurement of the plasma frequency of the doped semiconductor, following determination of the doping

https://doi.org/10.1021/acsenergylett.5c02283
ACS Energy Lett. 2025, 10, 4589−4595

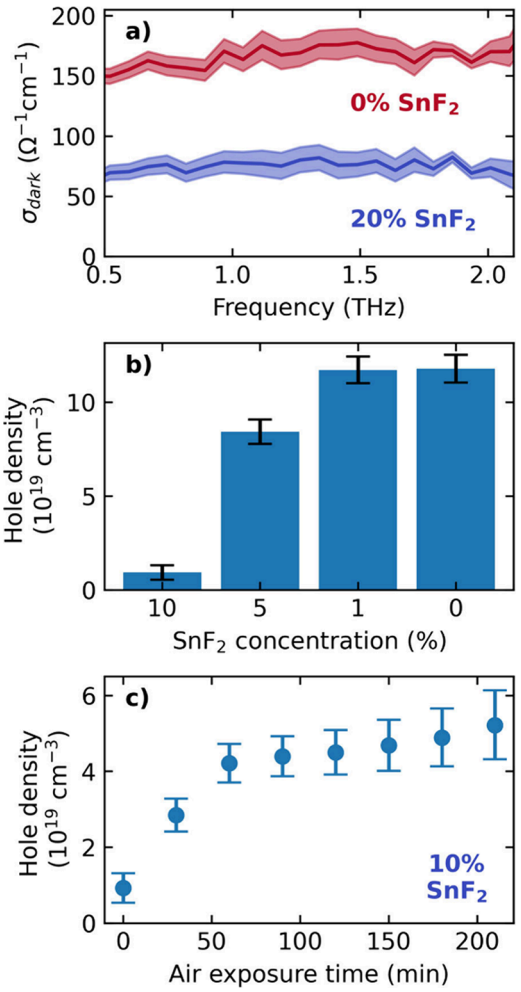

Figure 1. (a) THz dark conductivity spectra of $FASnI_3$ films processed with 0% and 20% SnF_2 additive. (b) Derived hole density in $FASnI_3$ films with 10%, 5%, 1% and 0% SnF_2 additive. (c) Hole density in $FASnI_3$ film (with 10% SnF_2 additive) as a function of increasing time in ambient air (temperature: 19 °C; ambient humidity: 45%).

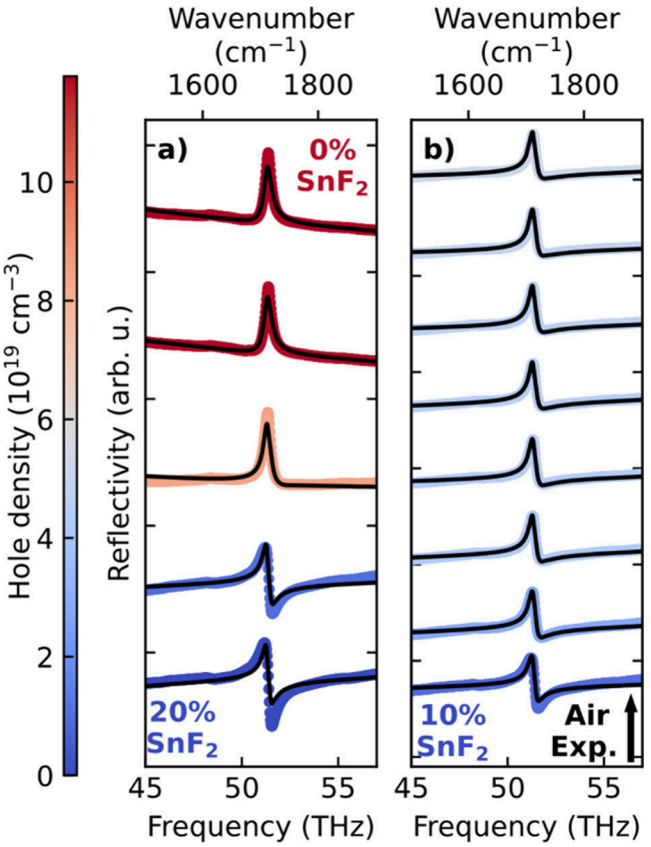

Figure 2. Reflectance spectra as a function of IR frequency ν for $FASnI_3$ films with (a) different amounts of SnF_2 additive and (b) 10% SnF_2 additive and air exposure time increasing from 0 to 210 min, in steps of 30 min. As previously shown,[28] air-exposure over the first 300 min has the predominant effect of increasing hole doping, with secondary-phase formation only commencing at longer times. Plots focus on the CN stretching mode of the FA cation. Black lines correspond to fits based on eq 1. Note that the x-axis reflects standard frequency ν while eq 1 and the plasma frequency are given in terms of angular frequency $\omega = 2\pi\nu$, as conventional.

density from Hall effect measurements.[15,47] However, for thin films, application of this method is practically hampered, in particular for tin-halide perovskites for which thin-films absorption features are particularly broad, thus hindering the clean observation of a plasma edge.[35] We posit here that by investigating changes in the line shape of IR-frequency vibrations of the organic FA cation as the plasma frequency sweeps through the vibrational peaks, we can accurately determine the plasma frequency. Here, we model the dielectric function of a doped semiconductor hosting a vibrational mode as a sum of a plasma response and a Lorentz oscillator term:[48,49]

$$\epsilon = \epsilon_{\text{inf}}\left(1 - \frac{\omega_p^2}{\omega^2 + i\omega\Gamma}\right) + \frac{A^2}{\omega_{FA}^2 - \omega^2 - i\omega\Gamma_{FA}} \quad (1)$$

where ω is the angular frequency (with $\omega = 2\pi\nu$, and ν being the frequency of the incident light indicated on the x-axes of Figure 2a,b), ϵ_{inf} is the dielectric constant at infinite angular frequency (with respect to the observation window), ω_p is the plasma frequency, Γ and Γ_{FA} are the broadening factors for the charge-carriers plasma and the FA vibrational mode, respectively, A is the oscillator strength of the vibration, and ω_{FA} is the angular frequency of the FA internal vibrational mode. The plasma frequency is defined by $\omega_p^2 = pe^2/\epsilon_0\epsilon_{inf}m_{eff}$, where is the doping density, ϵ_0 is the vacuum permittivity, and m_{eff} is the effective mass of the dopant charge carrier, i.e., the hole in this instance. Within this model, the reflectance line shape of the vibrational mode associated with a doped semiconductor is expected to change significantly, as demonstrated in Figure S6 which plots example solutions for eq 1. Such line shape change originates from the summation of the plasma mode and the Lorentz oscillator terms, with the phase of the overall dielectric constant markedly changing as the plasma frequency shifts through the frequency of the FA vibrational mode.

We find that for $FASnI_3$ films, such line shape changes can indeed be clearly observed for the CN stretching mode of the FA cation at ~ 1710 cm^{-1} as the hole density is varied (Figure 2a,b). We measured the spectral line shape in reflectance,[50] using the Fourier Transform Infrared (FTIR) technique, as detailed in SI Section 2.1. The line shape of the FA mode gradually but significantly changes as the hole density in the $FASnI_3$ films increases, either through decreases in SnF_2

https://doi.org/10.1021/acsenergylett.5c02283
ACS Energy Lett. 2025, 10, 4589−4595

concentrations (20, 10, 5, 1 and 0%, as shown in Figure 2a) or when $FASnI_3$ films are exposed to air (Figure 2b for a $FASnI_3$ film with 10% SnF_2 addition) which induces finely tuned changes in hole density. We have fitted these reflectance spectra based on the dielectric function captured by eq 1 with the resulting fits shown as black lines in Figure 2a,b. Here, for increased accuracy, the parameters ϵ_{inf}, Γ, A, ω_0, and Γ_{ph} were only allowed to vary globally and solely ω_p and a linear background term were permitted to vary between different spectra (see SI Section 3 for further details and discussion of the linear background term arising from minor variations between reflection from the substrate and surface scattering from different films). The resulting values extracted for the global parameters are shown in Table S1 in the SI. We briefly comment on the extracted value of $\epsilon_{inf} = 8.0 \pm 0.9$, which is in good agreement with literature reports ranging between 6.6 and 8.85.[37,40,41] We note that the term ϵ_{inf} can be somewhat ambiguous depending on the high-frequency limit of which resonance it refers to, with common usage referring to the near-IR range immediately below the electronic bandgap.[51] Our study focuses on molecular vibrational modes of the FA cation in the mid-IR range. Such vibrational modes in the mid- to near-IR range have been shown to only contribute marginally to the overall dielectric function,[52,53] and hence our value of ϵ_{inf} is similar to but slightly at the higher side of commonly reported values.

We further note that, intriguingly, the line shapes we report here resemble those for a Fano resonance,[54] a phenomenon arising from interference between a background of continuum states and a resonant (discrete) scattering process. This phenomenon is caused by weak coupling between the continuum and discrete states, and is revealed as a characteristic asymmetric line shape in either absorption or reflection spectra.[54,55] The Fano resonance line shape depends on the ratio of scattering between the two states, characterized by the Fano parameter q.[56] Assigning the observed reflectance response and their evolution with hole density to a Fano resonance with varying Fano parameter q would imply that a direct coupling exists between the hole plasma (the continuum) and the CN stretch mode (the discrete state).[54] Interestingly, there have been some reports of coupling between charge carriers and internal A-cation modes, possibly mediated by lead-halide cage modes,[57,58] and therefore such Fano resonance cannot be fully ruled out. However, our model captured by eq 1, which simply sums the plasma and oscillator responses to describe the dielectric function, will hold regardless of the presence of a Fano resonance. While a Fano-type resonance could, in principle, contribute as a further term to this approach, we note that our model already describes the experimental reflectance spectra very well, even without such an addition. We therefore conclude that any direct coupling between holes and internal A-cation modes can be only of relatively minor magnitude.

The square of the plasma frequency extracted from these fits shows a linear dependence on the hole density p (see Figure 3), as expected from the relation $\omega_p^2 = pe^2/\epsilon_0\epsilon_{inf}m_{eff}$.[59] The clear passage through the origin further supports our assumption of comparatively negligible hole densities encountered in the $FASnI_3$ thin film with 20% SnF_2 addition. Moreover, the linear behavior demonstrates that the parabolic approximation holds (i.e., constant mass) for the valence band of $FASnI_3$ even at doping densities as high as 10^{20} cm^{-3} for which the valence band will be significantly depleted (within

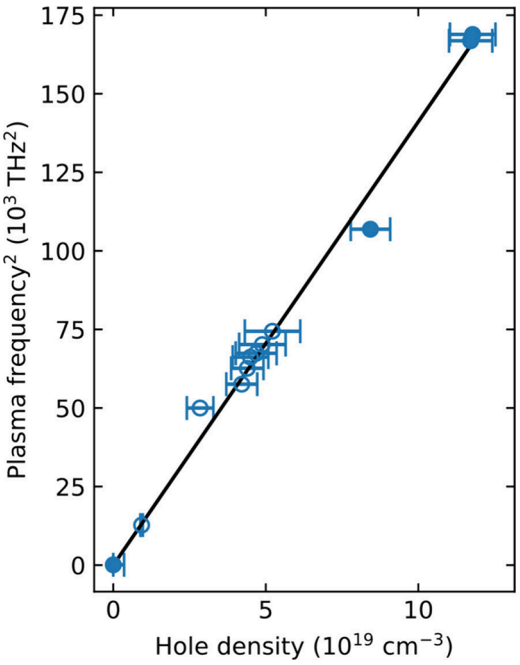

Figure 3. Square of the (angular) plasma frequency plotted as a function of the hole density, obtained from fits shown in Figure 2a,b, which demonstrates a linear dependence indicative of parabolic bands. Hollow circles correspond to data derived from the $FASnI_3$ film with 10% SnF_2 additive measured after different amount of air exposure (as shown in Figure 2b), and solid circles correspond to $FASnI_3$ films with different amounts of SnF_2 addition (as shown in Figure 2a).

the order of 100 meV at these doping densities[20]). We are thus able to extract the hole effective mass of $m_h^* = 0.28 \pm 0.05m_e$ from linear fits to these data with good accuracy. We note that this value is at the higher end of the range of typical predictions reported for computational calculations of the hole mass in $ASnX_3$ perovskites ($m_h^* = 0.1-0.3m_e$),[22,36−41] which underlines the need for experimental findings. We further note that our values are comparable to the effective hole mass of around $m_h^* = 0.2-0.3m_e$ deduced from bandstructure calculations and angle-resolved photoelectron spectroscopy for lead-halide perovskites.[22,60−62]

Our experimentally determined hole effective mass value for $FASnI_3$ has clear implications on the current understanding of charge-carrier transport in tin-iodide perovskites. A lower effective mass of charge carriers in tin-halide perovskites, obtained from first-principles simulations, has generally been quoted as the reason for higher mobilities in tin-halide perovskites compared to lead-halide perovskites.[29,45] However, our results suggest that other factors, such as coupling of charge carriers to phonons, may be responsible for the higher mobility. Within the Fröhlich model, the charge-carrier mobility is inversely proportional to the coupling coefficient $\alpha = \epsilon_{Fr}^{-1}(Ry/\hbar\omega_{LO})^{1/2}(m^*/m_e)^{1/2}$, where ω_{LO} is the LO phonon frequency, Ry = 13.606 eV the Rydberg constant, and $\epsilon_{Fr}^{-1} = \epsilon_{inf}^{-1} - \epsilon_{static}^{-1}$.[29,51] Factors other than the charge-carrier masses may therefore affect mobilities; for example, the lighter B-cation in tin-halide perovskites (compared to their lead-based counterparts) may lead to higher values of ω_{LO} and lower Fröhlich parameter α. In addition, any changes in the polar nature of the tin-halide bond may also be a factor. We note that some dependence of electron−phonon coupling on doping density

https://doi.org/10.1021/acsenergylett.5c02283
ACS Energy Lett. 2025, 10, 4589−4595

has been reported,[46] however our linear dependence of plasma frequency on doping density suggests that we are in the Drude regime associated with a free-charge response. We further note that some of the earlier reports[18] of tin iodide perovskites exhibiting room temperature mobilities of several hundred or thousand $cm^2/(Vs)$ in single-crystal specimens have not been repeatable for thin films.[20] Such differences may partly arise from inaccuracies arising when combining Hall coefficient and resistivity measurements across different specimens, and partly be related to heavy doping leading to a reduction in charge-carrier mobility as a result of carrier−carrier scattering and interactions with ionised impurities (e.g., tin vacancies).[20,29,63] As such, charge-carrier mobility values reported for thin films of tin- and lead-iodide perovskites are therefore often ultimately found to be within the same order of magnitude,[20,28] i.e. a few tens of $cm^2/(V\ s)$.

In conclusion, our study reports the hole effective mass of $FASnI_3$ thin films determined experimentally through non-contact optical spectroscopy. Our work utilizes a $FASnI_3$ thin film series with finely controllable hole density, which is tuned by either changes in the SnF_2 additive concentration during film fabrication or by exposing the film to the air to induce further tin vacancy formation and oxidation. We quantify the hole density through an all-optical approach by combining optical conductivity measurements from THz-TDS and mobility measurements from OPTP. We further determined the plasma frequency accurately by monitoring the IR reflectivity spectra across the frequency range of an internal vibrational mode of the FA cation. As the plasma frequency is swept past the resonance of the sharp FA mode with increasing hole density, clear changes to the line shape are observed and modeled based on a combined dielectric function capturing both the plasma and the molecular response. From the extracted plasma frequencies, we were able to determine a hole effective mass of $0.28 \pm 0.05 m_e$ for $FASnI_3$. This value appears similar to that reported for lead-halide perovskites, suggesting that any potential differences in mobilities may ultimately arise from changes in electron−phonon coupling. In addition, we note that our simple model highlights the absence of a Fano resonance in these spectra, i.e. any direct coupling between the continuum of hole states and the sharp A-cation molecular resonance appears to be insignificant. Overall, our results provide novel fundamental insight into the electronic properties of tin-halide perovskites, which currently offer the most promising photovoltaic performance within the emerging group of lead-free metal halide semiconductors.

■ ASSOCIATED CONTENT

Supporting Information

The Supporting Information is available free of charge at https://pubs.acs.org/doi/10.1021/acsenergylett.5c02283.

Sample fabrication details, experimental details of spectroscopic techniques and further characterization data, including mid-IR reflectance and optical absorption, terahertz time-domain spectroscopy (THz-TDS), optical-pump terahertz-probe (OPTP) photoconductivity spectroscopy, details on determination of background hole density, fitting methodology for IR reflectivity spectra, and parameters extracted from fits (PDF)

■ AUTHOR INFORMATION

Corresponding Author

Laura M. Herz − *Department of Physics, Clarendon Laboratory, University of Oxford, Oxford OX1 3PU, U.K.*; orcid.org/0000-0001-9621-334X; Email: laura.herz@physics.ox.ac.uk

Authors

Vincent J.-Y. Lim − *Department of Physics, Clarendon Laboratory, University of Oxford, Oxford OX1 3PU, U.K.*; orcid.org/0000-0002-9726-0436

Marcello Righetto − *Department of Physics, Clarendon Laboratory, University of Oxford, Oxford OX1 3PU, U.K.*; orcid.org/0000-0001-5507-1445

Michael D. Farrar − *Department of Physics, Clarendon Laboratory, University of Oxford, Oxford OX1 3PU, U.K.*

Thomas Siday − *School of Physics and Astronomy, University of Birmingham, Birmingham B15 2TT, U.K.*; orcid.org/0000-0003-0157-3233

Henry J. Snaith − *Department of Physics, Clarendon Laboratory, University of Oxford, Oxford OX1 3PU, U.K.*; orcid.org/0000-0001-8511-790X

Michael B. Johnston − *Department of Physics, Clarendon Laboratory, University of Oxford, Oxford OX1 3PU, U.K.*; orcid.org/0000-0002-0301-8033

Complete contact information is available at: https://pubs.acs.org/10.1021/acsenergylett.5c02283

Notes

The authors declare the following competing financial interest(s): H.J.S. is co-founder and CSO of Oxford PV Ltd., a company commercializing perovskite PV technology.

■ ACKNOWLEDGMENTS

The authors gratefully acknowledge financial support from the Engineering and Physical Sciences Research Council (EPSRC) UK. V.J.-Y.L. acknowledges financial support from an EPSRC Doctoral Prize.

■ REFERENCES

(1) De Angelis, F. The Prospect of Lead-Free Perovskite Photovoltaics. *ACS Energy Lett.* **2021**, *6* (4), 1586−1587.

(2) Ahmed, S.; Gondal, M. A.; Alzahrani, A. S.; Parvaz, M.; Ahmed, A.; Hussain, S. Recent Trends and Challenges in Lead-Free Perovskite Solar Cells: A Critical Review. *ACS Appl. Energy Mater.* **2024**, *7* (4), 1382−1397.

(3) Cheng, P.; Han, K.; Chen, J. Recent Advances in Lead-Free Halide Perovskites for Photocatalysis. *ACS Mater. Lett.* **2023**, *5* (1), 60−78.

(4) Dubey, A.; Sanchez, S. L.; Yang, J.; Ahmadi, M. Lead-Free Halide Perovskites for Photocatalysis via High-Throughput Exploration†. *Chem. Mater.* **2024**, *36* (5), 2165−2176.

(5) Zhou, Z.; Li, Q.; Chen, M.; Zheng, X.; Wu, X.; Lu, X.; Tao, S.; Zhao, N. High-Mobility and Bias-Stable Field-Effect Transistors Based on Lead-Free Formamidinium Tin Iodide Perovskites. *ACS Energy Lett.* **2023**, *8* (10), 4496−4505.

(6) Xiao, Z.; Meng, W.; Wang, J.; Mitzi, D. B.; Yan, Y. Searching for Promising New Perovskite-Based Photovoltaic Absorbers: The Importance of Electronic Dimensionality. *Mater. Horizons* **2017**, *4* (2), 206−216.

(7) Xiao, Z.; Song, Z.; Yan, Y. From Lead Halide Perovskites to Lead-Free Metal Halide Perovskites and Perovskite Derivatives. *Adv. Mater.* **2019**, *31* (47), 1803792.

(8) Jang, W. J.; Jang, H. W.; Kim, S. Y. Recent Advances in Wide Bandgap Perovskite Solar Cells: Focus on Lead-Free Materials for Tandem Structures. *Small Methods* **2024**, *8* (2), 2300207.
(9) Gu, S.; Lin, R.; Han, Q.; Gao, Y.; Tan, H.; Zhu, J. Tin and Mixed Lead-Tin Halide Perovskite Solar Cells: Progress and Their Application in Tandem Solar Cells. *Adv. Mater.* **2020**, *32* (27), 1907392.
(10) Yoon, S.; Ryu, J.; Cho, S. W.; Kim, H. Do; Lim, J.; Cho, J. S.; Park, J.; Kang, D. W. Lead-Free, Sn-Based All-Perovskite Tandem Solar Cells with an Efficiency Over 15%. *Small* **2025**, 2501876.
(11) Luo, J.; Wang, X.; Li, S.; Liu, J.; Guo, Y.; Niu, G.; Yao, L.; Fu, Y.; Gao, L.; Dong, Q.; Zhao, C.; Leng, M.; Ma, F.; Liang, W.; Wang, L.; Jin, S.; Han, J.; Zhang, L.; Etheridge, J.; Wang, J.; Yan, Y.; Sargent, E. H.; Tang, J. Efficient and Stable Emission of Warm-White Light from Lead-Free Halide Double Perovskites. *Nat. 2018 5637732* **2018**, *563* (7732), 541−545.
(12) Sharif, R.; Khalid, A.; Ahmad, S. W.; Rehman, A.; Qutab, H. G.; Akhtar, H. H.; Mahmood, K.; Afzal, S.; Saleem, F. A Comprehensive Review of the Current Progresses and Material Advances in Perovskite Solar Cells. *Nanoscale Adv.* **2023**, *5* (15), 3803−3833.
(13) Pitaro, M.; Tekelenburg, E. K.; Shao, S.; Loi, M. A. Tin Halide Perovskites: From Fundamental Properties to Solar Cells. *Adv. Mater.* **2022**, *34* (1), 2105844.
(14) Wang, L.; Bi, H.; Liu, J.; Wei, Y.; Zhang, Z.; Chen, M.; Baranwal, A. K.; Kapil, G.; Kitamura, T.; Yang, S.; Miao, Q.; Shen, Q.; Ma, T.; Hayase, S. Exceeding 15% Performance with Energy Level Tuning in Tin-Based Perovskite Solar Cells. *ACS Energy Lett.* **2024**, *9* (12), 6238−6244.
(15) Mitzi, D. B.; Feild, C. A.; Schlesinger, Z.; Laibowitz, R. B. Transport, Optical, and Magnetic Properties of the Conducting Halide Perovskite $CH_3NH_3SnI_3$. *J. Solid State Chem.* **1995**, *114* (1), 159−163.
(16) Takahashi, Y.; Hasegawa, H.; Takahashi, Y.; Inabe, T. Hall Mobility in Tin Iodide Perovskite $CH_3NH_3SnI_3$: Evidence for a Doped Semiconductor. *J. Solid State Chem.* **2013**, *205*, 39−43.
(17) Chung, I.; Song, J. H.; Im, J.; Androulakis, J.; Malliakas, C. D.; Li, H.; Freeman, A. J.; Kenney, J. T.; Kanatzidis, M. G. $CsSnI_3$: Semiconductor or Metal? High Electrical Conductivity and Strong near-Infrared Photoluminescence from a Single Material. High Hole Mobility and Phase-Transitions. *J. Am. Chem. Soc.* **2012**, *134* (20), 8579−8587.
(18) Stoumpos, C. C.; Malliakas, C. D.; Kanatzidis, M. G. Semiconducting Tin and Lead Iodide Perovskites with Organic Cations: Phase Transitions, High Mobilities, and near-Infrared Photoluminescent Properties. *Inorg. Chem.* **2013**, *52* (15), 9019−9038.
(19) Kamaraki, C.; Klug, M. T.; Lim, V. J. Y.; Zibouche, N.; Herz, L. M.; Islam, M. S.; Case, C.; Miranda Perez, L. Charting the Irreversible Degradation Modes of Low Bandgap Pb-Sn Perovskite Compositions for De-Risking Practical Industrial Development. *Adv. Energy Mater.* **2024**, *14* (10), 2302916.
(20) Milot, R. L.; Klug, M. T.; Davies, C. L.; Wang, Z.; Kraus, H.; Snaith, H. J.; Johnston, M. B.; Herz, L. M. The Effects of Doping Density and Temperature on the Optoelectronic Properties of Formamidinium Tin Triiodide Thin Films. *Adv. Mater.* **2018**, *30* (44), 1804506.
(21) Noel, N. K.; Stranks, S. D.; Abate, A.; Wehrenfennig, C.; Guarnera, S.; Haghighirad, A. A.; Sadhanala, A.; Eperon, G. E.; Pathak, S. K.; Johnston, M. B.; Petrozza, A.; Herz, L. M.; Snaith, H. J. Lead-Free Organic-Inorganic Tin Halide Perovskites for Photovoltaic Applications. *Energy Environ. Sci.* **2014**, *7* (9), 3061−3068.
(22) Umari, P.; Mosconi, E.; De Angelis, F. Relativistic GW Calculations on $CH_3NH_3PbI_3$ and $CH_3NH_3SnI_3$ Perovskites for Solar Cell Applications. *Sci. Rep.* **2014**, *4* (1), 4467.
(23) López-Fernández, I.; Valli, D.; Wang, C. Y.; Samanta, S.; Okamoto, T.; Huang, Y. T.; Sun, K.; Liu, Y.; Chirvony, V. S.; Patra, A.; Zito, J.; De Trizio, L.; Gaur, D.; Sun, H. T.; Xia, Z.; Li, X.; Zeng, H.; Mora-Seró, I.; Pradhan, N.; Martínez-Pastor, J. P.; Müller-Buschbaum, P.; Biju, V.; Debnath, T.; Saliba, M.; Debroye, E.; Hoye, R. L. Z.; Infante, I.; Manna, L.; Polavarapu, L. Lead-Free Halide Perovskite Materials and Optoelectronic Devices: Progress and Prospective. *Adv. Funct. Mater.* **2024**, *34* (6), 2307896.
(24) Li, X. Z.; Ye, Y.; Cao, Y.; Zhang, D.; Lin, Y.; Chang, J.; Zhu, L.; Wang, N.; Huang, W.; Wang, J. Tin-Halide Perovskites for Light-Emitting Diodes. *Chem. Soc. Rev.* **2025**, *54* (14), 6697−6725.
(25) Even, J.; Pedesseau, L.; Jancu, J. M.; Katan, C. DFT and K·p Modelling of the Phase Transitions of Lead and Tin Halide Perovskites for Photovoltaic Cells. *Phys. status solidi - Rapid Res. Lett.* **2014**, *8* (1), 31−35.
(26) Meggiolaro, D.; Ricciarelli, D.; Alasmari, A. A.; Alasmary, F. A. S.; De Angelis, F. Tin versus Lead Redox Chemistry Modulates Charge Trapping and Self-Doping in Tin/Lead Iodide Perovskites. *J. Phys. Chem. Lett.* **2020**, *11* (9), 3546−3556.
(27) Leijtens, T.; Prasanna, R.; Gold-Parker, A.; Toney, M. F.; McGehee, M. D. Mechanism of Tin Oxidation and Stabilization by Lead Substitution in Tin Halide Perovskites. *ACS Energy Lett.* **2017**, *2* (9), 2159−2165.
(28) Lim, V. J. Y.; Ulatowski, A. M.; Kamaraki, C.; Klug, M. T.; Miranda Perez, L.; Johnston, M. B.; Herz, L. M. Air-Degradation Mechanisms in Mixed Lead-Tin Halide Perovskites for Solar Cells. *Adv. Energy Mater.* **2023**, *13* (33), 2200847.
(29) Savill, K. J.; Ulatowski, A. M.; Herz, L. M. Optoelectronic Properties of Tin-Lead Halide Perovskites. *ACS Energy Lett.* **2021**, *6* (7), 2413−2426.
(30) Li, B.; Chang, B.; Pan, L.; Li, Z.; Fu, L.; He, Z.; Yin, L. Tin-Based Defects and Passivation Strategies in Tin-Related Perovskite Solar Cells. *ACS Energy Lett.* **2020**, *5* (12), 3752−3772.
(31) Yao, H.; Zhou, F.; Li, Z.; Ci, Z.; Ding, L.; Jin, Z. Strategies for Improving the Stability of Tin-Based Perovskite ($ASnX_3$) Solar Cells. *Adv. Sci.* **2020**, *7* (10), 1903540.
(32) Savill, K. J.; Ulatowski, A. M.; Farrar, M. D.; Johnston, M. B.; Snaith, H. J.; Herz, L. M. Impact of Tin Fluoride Additive on the Properties of Mixed Tin-Lead Iodide Perovskite Semiconductors. *Adv. Funct. Mater.* **2020**, *30* (52), 2005594.
(33) Treglia, A.; Ambrosio, F.; Martani, S.; Folpini, G.; Barker, A. J.; Albaqami, M. D.; De Angelis, F.; Poli, I.; Petrozza, A. Effect of Electronic Doping and Traps on Carrier Dynamics in Tin Halide Perovskites. *Mater. Horizons* **2022**, *9* (6), 1763−1773.
(34) Galkowski, K.; Mitioglu, A.; Miyata, A.; Plochocka, P.; Portugall, O.; Eperon, G. E.; Wang, J. T. W.; Stergiopoulos, T.; Stranks, S. D.; Snaith, H. J.; Nicholas, R. J. Determination of the Exciton Binding Energy and Effective Masses for Methylammonium and Formamidinium Lead Tri-Halide Perovskite Semiconductors. *Energy Environ. Sci.* **2016**, *9* (3), 962−970.
(35) Galkowski, K.; Surrente, A.; Baranowski, M.; Zhao, B.; Yang, Z.; Sadhanala, A.; Mackowski, S.; Stranks, S. D.; Plochocka, P. Excitonic Properties of Low-Band-Gap Lead-Tin Halide Perovskites. *ACS Energy Lett.* **2019**, *4* (3), 615−621.
(36) Kahmann, S.; Nazarenko, O.; Shao, S.; Hordiichuk, O.; Kepenekian, M.; Even, J.; Kovalenko, M. V.; Blake, G. R.; Loi, M. A. Negative Thermal Quenching in $FASnI_3$ Perovskite Single Crystals and Thin Films. *ACS Energy Lett.* **2020**, *5* (8), 2512−2519.
(37) Roknuzzaman, M.; Alarco, J. A.; Wang, H.; Du, A.; Tesfamichael, T.; Ostrikov, K. K. Ab Initio Atomistic Insights into Lead-Free Formamidinium Based Hybrid Perovskites for Photovoltaics and Optoelectronics. *Comput. Mater. Sci.* **2019**, *169*, 109118.
(38) Yu, Z. L.; Ma, Q. R.; Zhao, Y. Q.; Liu, B.; Cai, M. Q. Surface Termination - A Key Factor to Influence Electronic and Optical Properties of $CsSnI_3$. *J. Phys. Chem. C* **2018**, *122* (17), 9275−9282.
(39) Jiang, J.; Onwudinanti, C. K.; Hatton, R. A.; Bobbert, P. A.; Tao, S. Stabilizing Lead-Free All-Inorganic Tin Halide Perovskites by Ion Exchange. *J. Phys. Chem. C* **2018**, *122* (31), 17660−17667.
(40) Peng, L.; Xie, W. Theoretical and Experimental Investigations on the Bulk Photovoltaic Effect in Lead-Free Perovskites $MASnI_3$ and $FASnI_3$. *RSC Adv.* **2020**, *10* (25), 14679−14688.
(41) Feng, J.; Xiao, B. Effective Masses and Electronic and Optical Properties of Nontoxic $MASnX_3$ (X = Cl, Br, and I) Perovskite

https://doi.org/10.1021/acsenergylett.5c02283
ACS Energy Lett. 2025, 10, 4589−4595

Structures as Solar Cell Absorber: A Theoretical Study Using HSE06. *J. Phys. Chem. C* **2014**, *118* (34), 19655−19660.
(42) Ban, H.; Zhang, T.; Gong, X.; Sun, Q.; Zhang, X. L.; Pootrakulchote, N.; Shen, Y.; Wang, M. Fully Inorganic $CsSnI_3$ Mesoporous Perovskite Solar Cells with High Efficiency and Stability via Coadditive Engineering. *Sol. RRL* **2021**, *5* (7), 2100069.
(43) Koh, T. M.; Krishnamoorthy, T.; Yantara, N.; Shi, C.; Leong, W. L.; Boix, P. P.; Grimsdale, A. C.; Mhaisalkar, S. G.; Mathews, N. Formamidinium Tin-Based Perovskite with Low Eg for Photovoltaic Applications. *J. Mater. Chem. A* **2015**, *3* (29), 14996−15000.
(44) Xiao, M.; Gu, S.; Zhu, P.; Tang, M.; Zhu, W.; Lin, R.; Chen, C.; Xu, W.; Yu, T.; Zhu, J. Tin-Based Perovskite with Improved Coverage and Crystallinity through Tin-Fluoride-Assisted Heterogeneous Nucleation. *Adv. Opt. Mater.* **2018**, *6* (1), 1700615.
(45) Poncé, S.; Schlipf, M.; Giustino, F. Origin of Low Carrier Mobilities in Halide Perovskites. *ACS Energy Lett.* **2019**, *4* (2), 456−463.
(46) Gatto, L.; Poli, I.; Meggiolaro, D.; Grandi, F.; Folpini, G.; Treglia, A.; Cinquanta, E.; Petrozza, A.; De Angelis, F.; Vozzi, C. Charge-Phonon Coupling in Tin Halide Perovskites. *ACS Energy Lett.* **2025**, *10* (3), 1382−1388.
(47) Schubert, E. F. *Doping in III-V Semiconductors*; Cambridge University Press: 1993.
(48) McMahon, T. J.; Bell, R. J. Infrared Reflectivity of Doped InSb and CdS. *Phys. Rev.* **1969**, *182* (2), 526.
(49) Shkerdin, G.; Rabbaa, S.; Stiens, J.; Vounckx, R. Influence of Electron Scattering on Phonon-Plasmon Coupled Modes Dispersion and Free-Electron Absorption in n-Doped GaN Semiconductors at Mid-IR Wavelengths. *Phys. status solidi* **2014**, *251* (4), 882−891.
(50) Tejada, A.; Peters, S.; Al-Ashouri, A.; Turren-Cruz, S. H.; Abate, A.; Albrecht, S.; Ruske, F.; Rech, B.; Guerra, J. A.; Korte, L. Hybrid Perovskite Degradation from an Optical Perspective: A Spectroscopic Ellipsometry Study from the Deep Ultraviolet to the Middle Infrared. *Adv. Opt. Mater.* **2022**, *10* (3), 2101553.
(51) Herz, L. M. How Lattice Dynamics Moderate the Electronic Properties of Metal-Halide Perovskites. *J. Phys. Chem. Lett.* **2018**, *9* (23), 6853−6863.
(52) Pérez-Osorio, M. A.; Milot, R. L.; Filip, M. R.; Patel, J. B.; Herz, L. M.; Johnston, M. B.; Giustino, F. Vibrational Properties of the Organic-Inorganic Halide Perovskite $CH_3NH_3PbI_3$ from Theory and Experiment: Factor Group Analysis, First-Principles Calculations, and Low-Temperature Infrared Spectra. *J. Phys. Chem. C* **2015**, *119* (46), 25703−25718.
(53) Glaser, T.; Müller, C.; Sendner, M.; Krekeler, C.; Semonin, O. E.; Hull, T. D.; Yaffe, O.; Owen, J. S.; Kowalsky, W.; Pucci, A.; Lovrinčić, R. Infrared Spectroscopic Study of Vibrational Modes in Methylammonium Lead Halide Perovskites. *J. Phys. Chem. Lett.* **2015**, *6* (15), 2913−2918.
(54) Fano, U. Effects of Configuration Interaction on Intensities and Phase Shifts. *Phys. Rev.* **1961**, *124* (6), 1866.
(55) Limonov, M. F.; Rybin, M. V.; Poddubny, A. N.; Kivshar, Y. S. Fano Resonances in Photonics. *Nat. Photonics* **2017**, *11* (9), 543−554.
(56) Iizawa, M.; Kosugi, S.; Koike, F.; Azuma, Y. The Quantum and Classical Fano Parameter Q. *Phys. Scr.* **2021**, *96* (5), 055401.
(57) Grechko, M.; Bretschneider, S. A.; Vietze, L.; Kim, H.; Bonn, M. Vibrational Coupling between Organic and Inorganic Sublattices of Hybrid Perovskites. *Angew. Chemie Int. Ed.* **2018**, *57* (41), 13657−13661.
(58) Man, G. J.; Kamal, C.; Kalinko, A.; Phuyal, D.; Acharya, J.; Mukherjee, S.; Nayak, P. K.; Rensmo, H.; Odelius, M.; Butorin, S. M. A-Site Cation Influence on the Conduction Band of Lead Bromide Perovskites. *Nat. Commun.* **2022**, *13* (1), 1−10.
(59) Fox, A. M. *Optical Properties of Solids*; Oxford University Press: 2012.
(60) Yang, J.; Meissner, M.; Yamaguchi, T.; Zhang, X.; Ueba, T.; Cheng, L.; Ideta, S.; Tanaka, K.; Zeng, X.; Ueno, N.; Kera, S. Band Dispersion and Hole Effective Mass of Methylammonium Lead Iodide Perovskite. *Sol. RRL* **2018**, *2* (10), 1800132.
(61) Giorgi, G.; Fujisawa, J. I.; Segawa, H.; Yamashita, K. Small Photocarrier Effective Masses Featuring Ambipolar Transport in Methylammonium Lead Iodide Perovskite: A Density Functional Analysis. *J. Phys. Chem. Lett.* **2013**, *4* (24), 4213−4216.
(62) Bokdam, M.; Sander, T.; Stroppa, A.; Picozzi, S.; Sarma, D. D.; Franchini, C.; Kresse, G. Role of Polar Phonons in the Photo Excited State of Metal Halide Perovskites. *Sci. Rep.* **2016**, *6* (1), 1−8.
(63) Kumar, M. H.; Dharani, S.; Leong, W. L.; Boix, P. P.; Prabhakar, R. R.; Baikie, T.; Shi, C.; Ding, H.; Ramesh, R.; Asta, M.; Graetzel, M.; Mhaisalkar, S. G.; Mathews, N. Lead-Free Halide Perovskite Solar Cells with High Photocurrents Realized through Vacancy Modulation. *Adv. Mater.* **2014**, *26* (41), 7122−7127.

https://doi.org/10.1021/acsenergylett.5c02283
ACS Energy Lett. 2025, 10, 4589−4595